

UNIVERSITY OF TWENTE.

Faculty of Electrical Engineering,
Mathematics & Computer Science

Experimental Evaluation of Harmonic Tag Operation in the Presence of Multiple Transmitters

Twan Birnie
B.Sc. Thesis
July 1, 2022

Supervisors University of Twente:
dr.ir. Andre Kokkeler
dr.ing. Anastasia Lavrenko
dr.ir. Anne-Johan Annema

Radio Systems Group
Faculty of Electrical Engineering,
Mathematics and Computer Science
University of Twente
P.O. Box 217
7500 AE Enschede
The Netherlands

Summary

This report presents the results of an experimental study evaluating a mathematical model of harmonic tags used to create a nonlinear response in harmonic radar systems. Harmonic radar is a type of nonlinear radar. Instead of scanning on the transmit frequency for a return signal, with nonlinear radar the return signal is expected on another frequency. This typically requires a nonlinear element (active or passive). Harmonic radar uses a passive tag with a nonlinear element like a diode to create harmonics. Often the second harmonic is used since it has the most power. However, the harmonic return signal is still much weaker compared to the fundamental frequency. This results in a weak return signal which significantly limits the operational range of harmonic radar systems. Conventionally, increased transmit power, low sensitivity receivers, as well as high gain transmit and receive antennas are used to compensate. Recently, an alternative has been proposed that uses multiple lower power transmitters instead. The feasibility of this approach depends on the correctness of a mathematical model describing the harmonic tags that the multiple transmitter approach relies on. However, this mathematical model has not been experimentally verified yet. In this report, measurements with two transmitters are performed and compared against theoretical predictions based on the simulation results using the mathematical model. The results indicate that the mathematical model describes the behaviour of harmonic tags well in the entire input power range. The primary limitation of the model is that the power of the harmonic signal tends to be overestimated compared to the measurements. This leads to optimistic range estimations.

Contents

- 1 Introduction 4**
 - 1.1 Nonlinear radar 4
 - 1.2 Limitations of harmonic radar 5
 - 1.3 Research goals 5
 - 1.4 Outline 6

- 2 Harmonic Radar 7**
 - 2.1 Harmonic radar 7
 - 2.2 Mathematical model of a harmonic tag 8
 - 2.3 Auxiliary transmitters 9
 - 2.4 Model verification 10

- 3 Simulation results 11**
 - 3.1 Simulation setup 11
 - 3.2 Single transmitter power sweep 13
 - 3.3 Two transmitter power sweep 14

- 4 Measurements 17**
 - 4.1 Measurement setup 17
 - 4.2 Measurements with one transmitter 19
 - 4.3 Measurements with two transmitters 21
 - 4.4 Modulated carrier 26

- 5 Conclusion and Outlook 27**

- References 29**

Chapter 1

Introduction

1.1 Nonlinear radar

Nonlinear radar is a type of radar where instead of scanning for a return signal on the same frequency at which a radar signal is sent, the receiver scans for a return signal generated by a nonlinear target on a different frequency [1]. In nature, most objects will not create a nonlinear radar response, since they do not contain nonlinear elements. Therefore, by scanning on a different frequency from the radar signal, nonlinear radar can be used in cluttered environments for detecting targets that can create a nonlinear radar response that would not be detected by conventional radar [1]. However, there are still objects that can create a nonlinear response. For example in [2] the harmonics created by the nonlinearity of electronic circuits are used to try to detect hidden devices. The article also mentions other undesired sources of nonlinearities such as corrosive or junction metals.

An example of the application of nonlinear radar is given in [3], where nonlinear radar was used to map the flight patterns of butterflies. Furthermore, the company Recco has commercialized the application of nonlinear radar to locate people for search and rescue purposes [4].

The field of nonlinear radar is divided into three categories [1]. The first is subharmonic radar. Subharmonic radar uses an active tag with a frequency divider to create harmonics below the pilot frequency [1]. The second is harmonic radar. Harmonic radar uses active or passive tags with a nonlinear element to generate harmonics at multiples of the pilot frequency [1]. The final category is intermodulating radar. In intermodulating radar, two carrier frequencies are transmitted. An active or passive nonlinear tag mixes these frequencies, creating an intermodulating term between the two pilot frequencies [1]. The main difference between harmonic and intermodulating radar is the frequency composi-

tion of the transmit signal. Both harmonic and intermodulating radar tend to use the same types of nonlinear tags [1]. In this report, we consider both harmonic and intermodulating operating modes with passive tags, and hence refer to both as harmonic radar.

1.2 Limitations of harmonic radar

The disadvantage of harmonic radar systems is the poor power conversion from the radar signal to the harmonic at the tag. This results in a weak return signal, limiting the usable range of the harmonic radar system. The conventional solution to increase range is a combination of increased transmit power, low sensitivity receivers, and high gain transmit and receive antennas. This however leads to high power consumption, cost, and complexity [1].

As an alternative approach to increase range [5] proposes the use of multiple auxiliary transmitters. These auxiliary transmitters transmit an unmodulated carrier that combined with the radar signal at the tag increase the effective power output from the tag. A mathematical model derived in [5] and numerical simulations show that this could be a viable solution that could potentially even surpass the performance benefit of increased power output from a single transmitter.

These results depend on an accurate model of the harmonic tag. This mathematical model is derived in [6]. However, up until this point this model has not been verified with measurements.

1.3 Research goals

The research goal of this report is two-fold. The primary goal is to test the hypothesis formulated by the current mathematical model from [6] in a measurement setup with a real-life harmonic tag. The research question can thus be defined as:

1. *"How well does the mathematical model of a harmonic tag describe tag operation with multiple transmitters?"*

Secondly, it is important to evaluate what impact the measurement results have on the design of harmonic radar systems. Specifically with systems that use multiple transmitters in mind. The second research question is therefore:

2. *"How to design harmonic radar systems to best utilize a multiple transmitter configuration?"*

1.4 Outline

In this report, in Chapter 2 first more theory about harmonic radar is given and a mathematical model for the harmonic tag is explained. Then, a multiple transmitter setup is described and it is shown how it can be used to boost the return signal of a harmonic tag. This theory is used in Chapter 3 to formulate the test hypothesis for the measurements using simulation results. After this, in Chapter 4 the measurement setup is described, followed by the presentation of experimental results and their comparison with simulations. Finally, section 5 presents the conclusions and provides system design recommendations for harmonic radar systems that utilise multiple transmitters.

Chapter 2

Harmonic Radar

2.1 Harmonic radar

This report focuses on harmonic radar. Harmonic radar is based on receiving harmonics generated by a harmonic tag [1]. A simple passive harmonic tag consists of only an antenna, an inductive loop that functions as a matching circuit, and a diode as nonlinear element. A picture of such a passive harmonic tag can be seen in figure 2.1.

Consider a simple tone being picked up by the harmonic tag's antenna. When the sinusoidal current passes through the diode, an ideal diode would rectify the wave. This nonlinear behaviour introduces many harmonics, as seen in figure 2.2. This figure shows a pure sine wave that gets rectified by an ideal diode and the corresponding frequency spectrum. Here it can be seen that harmonics get generated at multiples of the original frequency.

Figure 2.2 also illustrates the main downside of harmonic radar: the poor power conversion at the tag from the radar signal to a harmonic. In figure 2.2, it can be seen that the power of the harmonics is lower than that of the radar frequency. This results in weak return signals and thus limited range. Furthermore the figure shows that higher harmonics

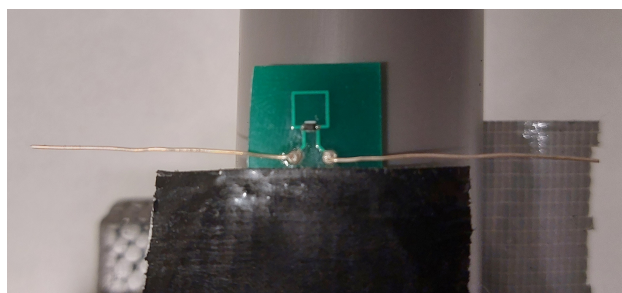


Figure 2.1: Harmonic tag close-up photo

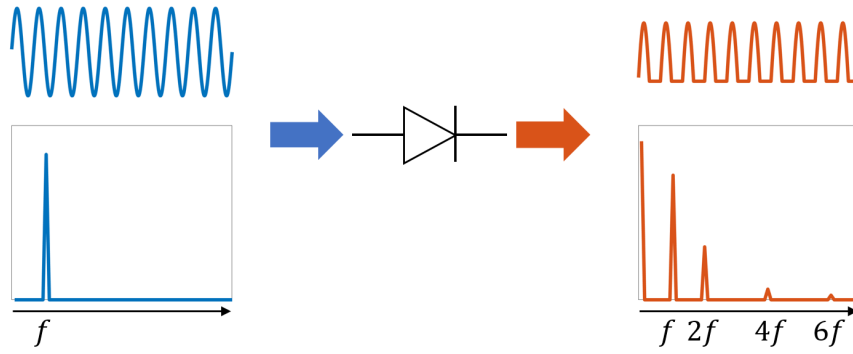


Figure 2.2: Simplified operation principle of harmonic tags

have less power. This is why the second harmonic is often used in harmonic radar, since it is the harmonic with the most power besides the first harmonic [1].

2.2 Mathematical model of a harmonic tag

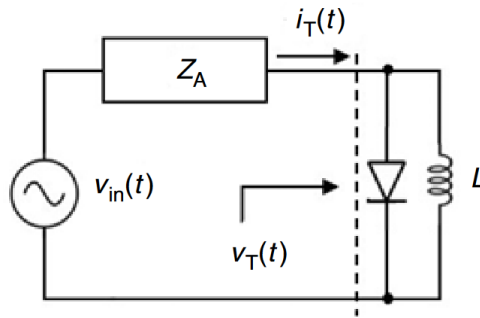


Figure 2.3: Simplified model of a harmonic tag, adopted from [6]

For analyzing harmonic radar systems, it is important to have a good model of harmonic tags. In [6] such a model has been derived using mathematical analysis with the Lambert W function. This model is based on the simplified model of the harmonic tag that can be seen in figure 2.3.

By assuming perfect impedance matching, the complex antenna input impedance Z_A is simplified to only a real impedance R_A . Furthermore it is assumed that the input bandwidth is sufficient for the bandwidth of the input signal. Using these assumptions, equation 2.1 was derived in [6] to describe the relation between the input voltage and the current through the diode.

$$i_T(t) = \left(\frac{W_0 \left(\rho e^{\rho + \tilde{v}_{in}(t)} \right)}{\rho} - 1 \right) I_S \quad (2.1)$$

In this equation W_0 is the principle branch of the Lambert W function, $\rho = \frac{I_S R_A}{n_i V_T}$ and $\tilde{v}_{in}(t) = \frac{v_{in}(t)}{n_i V_T}$. Here I_S is the saturation current of the diode, n_i the diodes ideality factor, V_T the thermal voltage (kT/q) and R_A the resistance of the antenna.

Furthermore, in [6] this model was analysed for two regions: a small signal and large signal region. For the small signal region using Taylor expansion it was found that the model shows a quadratic relation between the radar signal and the harmonic tag output at the second harmonic for both frequency and amplitude. For the large signal region, a quasi-linear relation was found. In this region, the model shows a quadratic relation between the frequency of the radar signal and the tag output at the second harmonic and a linear relation for amplitude.

2.3 Auxiliary transmitters

As shown in Section 2.1, harmonic radar suffers from poor power conversion at the tag. This results in limited range due to a weak return signal. Conventionally this has been solved by a combination of increased transmit power, low sensitivity receivers, and high gain transmit and receive antennas. However, both of these solutions result in heavy, complex, and expensive equipment [5]. Therefore, [5] proposes an alternative approach, which utilizes multiple transmitters.

In the proposed system, one transmitter would send the modulated radar signal and multiple auxiliary transmitters would transmit an unmodulated carrier that boosts the output of the tag. This usage of multiple transmitters can be seen as a combination of both harmonic radar and intermodulating radar. This is because while harmonic radar is still the basis of the system and tag design, the presence of an intermodulating term is exploited to allow the usage of multiple transmitters where only one of the transmitters modulates its signal.

In [5], the system was analyzed for the small signal region of the harmonic tag. In this region the relation between the input signal and the second harmonic is quadratic. The relation between the input voltage and the first two harmonics can be seen in equation 2.2 [5]. In this equation $\alpha = \frac{1}{n_i V_T}$.

$$i_T(t) = I_S \left(\alpha v(t) + \frac{\alpha^2}{2} v^2(t) \right) \quad (2.2)$$

When receiving multiple signals, the total input voltage will be the sum of these signals. For two signals $v_1(t)$ and $v_2(t)$ we can thus write:

$$i_T(t) = I_S \left(\alpha (v_1(t) + v_2(t)) + \frac{\alpha^2}{2} (v_1^2(t) + 2v_1(t)v_2(t) + v_2^2(t)) \right) \quad (2.3)$$

Furthermore, since we are only interested in the harmonics generated by the quadratic terms, we can leave out the linear terms to find:

$$i_T(t) = I_S \left(\frac{\alpha^2}{2} (v_1^2(t) + 2v_1(t)v_2(t) + v_2^2(t)) \right) \quad (2.4)$$

We can see that when two signals are applied at the input the result will be three harmonics at the output. The first and last terms are quadratic versions of the two input signals $v_1(t)$ and $v_2(t)$. The middle term is an intermodulating term between the two input signals. One can see that when $v_1(t)$ and $v_2(t)$ have the same amplitude, the intermodulating term has twice the amplitude compared to the harmonic terms, thus 6 dB more power.

Since doubling the transmit power also results in the same 6 dB gain, this does not result in an improvement compared to increasing the transmit power. However, using this effect allows for new designs for harmonic radar systems. Furthermore, since lower transmit powers are easier to achieve combined with the fact only one transmitter needs to modulate its output, it could allow for simpler, cheaper and lighter transmitters. To improve on the efficiency compared to doubling the output power, the intermodulating term and the harmonic of the modulated signal would have to be combined. This restricts the used modulation schemes to schemes where $x(t) = x^2(t)$.

2.4 Model verification

The results from Section 2.3 depend on the correctness of the mathematical model described in Section 2.2. However, this model has not yet been verified with measurements. This report will focus on verifying the mathematical model describing the operation of harmonic tags with lab measurements.

These measurements will be done using two transmitters that are swept over power levels. These measurements are enough to evaluate if the model as shown in equation 2.1 holds, since they are able to show the relation between the harmonics and intermodulating terms. Furthermore the transmitted signals will be simple tones instead of modulated signals. The simple tones are easier to generate and allow for easy and accurate measurements of the powers of the different harmonics.

In the end of the report, an example of a system with a modulated signal combined with an unmodulated signal will be shown, to give an impression of system operation similar to that of a practical setup.

Chapter 3

Simulation results

3.1 Simulation setup

To formulate the hypotheses for the measurements simulations were performed. Equation 2.1 was used as the basis for performing simulations. The values used to describe the harmonic tag can be seen in table 3.1. These values are based on the tag that will be used for measurements. The tag has been designed for operation at 2.9 GHz at the fundamental transmit frequency and 5.8 GHz at the harmonic return frequency [7]. The tag has a SkyWorks SMS7630-040 diode, whose specifications can be found in [8], with a dipole antenna that is 58 mm long and has a diameter of 0.38 mm. The resistance of this antenna was determined using the MATLAB Antenna Designer tool to be 142 Ohms at 2.9 GHz.

Parameter	Value
Saturation current I_s	$5 \cdot 10^{-6}$ A
Ideality parameter n_i	1.05
Thermal voltage V_T (at 21°C)	$25.2 \cdot 10^{-3}$ V
Coefficient ρ	0.0269

Table 3.1: Harmonic tag parameters

The simulations are done using MATLAB and consist of two parts. The first part is a time-domain simulation where the return signal from the harmonic tag is calculated. The second part transforms the time-domain signal to the frequency domain, to measure the power of the harmonics.

First, the input voltage at the tag needs to be calculated. The input voltage at the tag will be an unmodulated sine wave. The input voltage at the tag can be calculated using equation 3.1.

$$v_{in,t} = \sqrt{P_{tx,f_0} \cdot f_{spl} \cdot 2 \cdot 73 \cdot \sin(2 \cdot \pi \cdot f_0 \cdot t)} \quad (3.1)$$

Here P_{tx,f_0} is the transmit power in Watts and f_0 the frequency of the carrier. The equation for the free space path loss can be seen in equation 3.2 [9].

$$f_{spl} = G_{tx} G_{rx} \left(\frac{\lambda}{4\pi d} \right)^2 \quad (3.2)$$

In this equation G_{tx} and G_{rx} are the gains of the transmitting and receiving antenna, respectively. λ indicates the wavelength which was calculated from f_0 . d denotes the distance between the antenna and the tag. This equation is used twice: one time from the transmitting antenna to the harmonic tag and one time from the harmonic tag to the receiving antenna. For the transmitting and receiving antenna a gain of 6 dBi and 12 dBi from their specifications was used, respectively. For the antenna at the tag a gain of 2.15 dBi was used, typical for a half-wave dipole [10]. Both receiving and transmitting antenna's were at a distance of 0.2 meters from the tag.

From this calculated input voltage, the output current of the tag can be calculated using equation 2.1. This output current can then be converted to the output voltage using the antenna impedance. From this output voltage, the frequency spectrum is calculated using a Fast Fourier Transform (FFT), which is then normalised. The output of the normalised FFT is then converted to logarithmic scale. This output now represents the square peak voltage. To convert this to the actual power in dBm, the following relation is applied:

$$P_{rx} = \frac{V_{RMS}^2}{R} = \frac{V_{peak}^2}{2R} \quad (3.3)$$

Where V_{peak} is the amplitude of the sine wave and R the resistance. In logarithmic scale this operation can be achieved by subtracting $10 \log_{10}(2R)$ from the previously calculated logarithmic output. Finally, the free space path loss in logarithmic scale is added to account for the path loss and 30 dB is added to convert to dBm. Since the frequencies of the harmonics are already known, it is trivial to extract the amplitudes from the resulting frequency spectrum.

The range of power levels is chosen to be 10 dBm bigger in than the measurements. This will later be used to allow for the measurements to be compared to the simulations.

3.2 Single transmitter power sweep

The first simulation performed was with a single transmitter. The relation between the transmit power P_{tx,f_0} and the received power of the second harmonic $P_{rx,2f_0}$ was simulated. The frequency of the input signal was set to 2.9 GHz and swept from -20 dBm through 30 dBm. The result of this can be seen in figure 3.1a. Here, the quadratic and quasi-linear relation for the large signal and small signal regions described in [6] can be distinguished. From -20 dB to 5 dB, the line has a slope of 20 dB per decade, after which it starts to slope off. This can be seen more clearly in figure 3.1b. Here, the received harmonic power is plotted relative to the transmit power, and thus in the lower region has a slope of 10 dB per decade, which then starts to roll off.

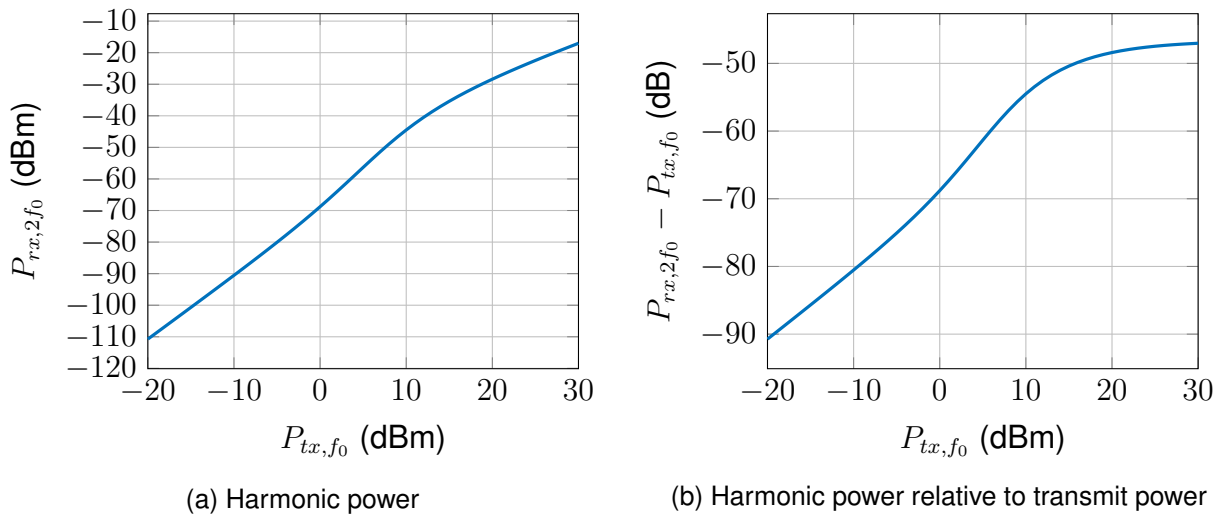


Figure 3.1: Simulated received harmonic power as a function of transmit power

3.3 Two transmitter power sweep

The second simulation uses two transmitters. The transmitters are set 10 KHz apart to $2.9e9 - 10e3 = 2.89999$ GHz and 2.9 GHz, respectively. A sweep was done from -20 dBm through 20 dBm with both transmitters at the same power level. The result of this sweep can be seen in figure 3.2a. In this figure, P_{rx} denotes the power received for both the harmonics ($P_{rx,2f_0}$ and $P_{rx,2f_1}$) or the intermodulating term (P_{rx,f_0+f_1}). P_{tx,f_0,f_1} denotes the transmit power of both transmitters. To better analyse the relation between the harmonics and the intermodulating term, figure 3.2b is plotted. It shows the received power of the two harmonics relative to the intermodulating term. It can be seen that for the lower transmit powers, the intermodulating term is indeed 6 dB higher than the harmonics, as predicted in Section 2.3. Furthermore, it shows that with increasing transmit power the gap between the harmonics and the intermodulating term first narrows before it widens again when the tag starts to approach the large signal quasi-linear region. This result is important since it shows that the intermodulating term is present across the entire range of input powers and at least 5 dB stronger than the other harmonics.

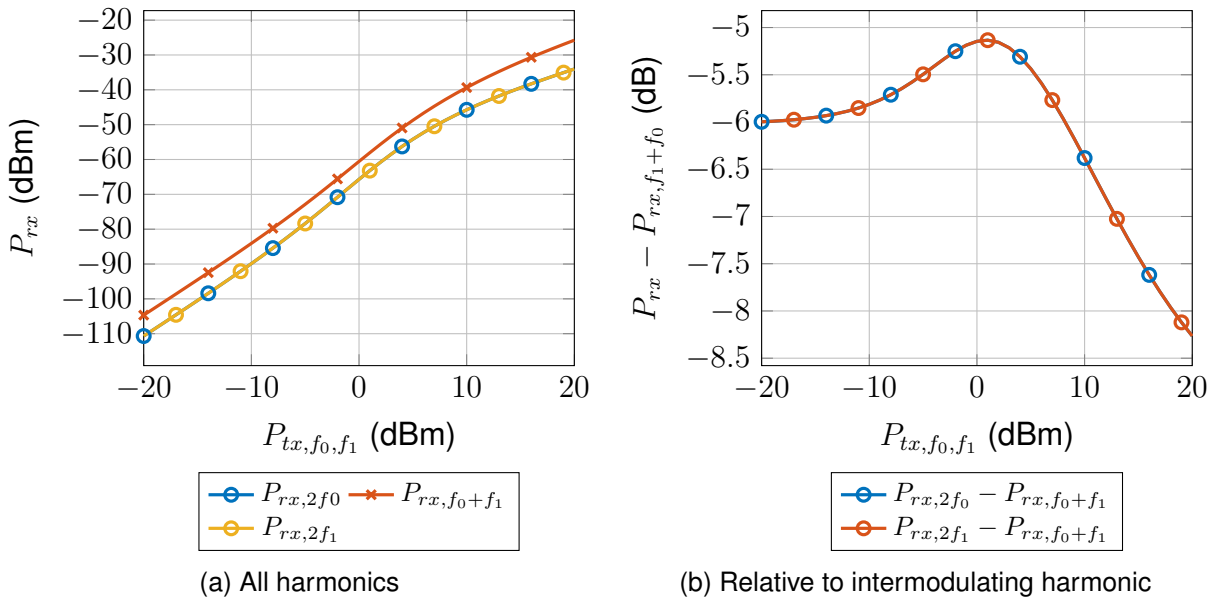
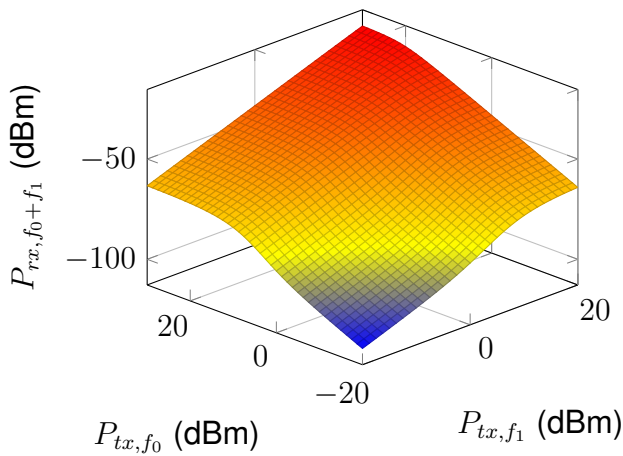


Figure 3.2: Simulated received harmonic power as a function of transmit power with two transmitters

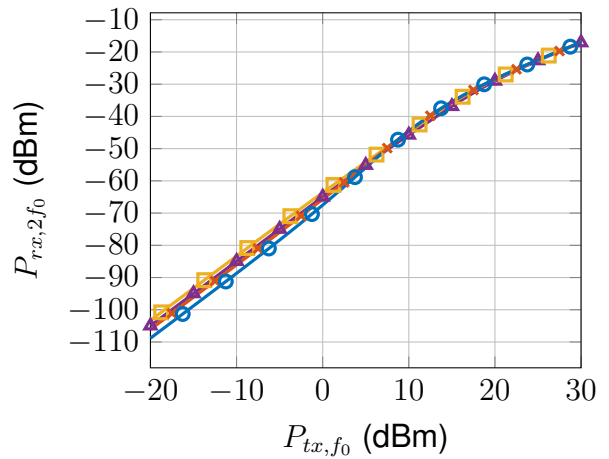
To expand on these results, simulations were also performed with unequal transmit power levels. These simulations were performed with the power level of both transmitters as two variables. One transmitter P_{tx,f_0} was swept from -20 dBm through 30 dBm and the other transmitter P_{tx,f_1} from -20 dBm through 20 dBm. This allows for plotting a 3D-figure as can be seen in figure 3.3a. In this figure the received signal power of the intermodulating term (P_{rx,f_0+f_1}) is plotted against the two transmit powers. While the surface looks as expected

from the mathematical model, it is difficult to accurately use the 3D-graph. Therefore, for the other plots it was chosen to plot slices of the 3D-graph. These can be seen in figures 3.3b, 3.3c, and 3.3d for the lower harmonic, intermodulating term and higher harmonic, respectively. In figure 3.3b, it can be seen that the harmonic power $P_{rx,2f_0}$ still behaves as expected from the power sweep with one transmitter. However, the other transmitter P_{tx,f_1} influences the power of the harmonic slightly. This can be better seen in figure 3.3d. Here the power of the harmonic of the second transmitter $P_{rx,2f_1}$ is plotted compared to the transmit power of the first transmitter P_{tx,f_0} . It can be seen that when the difference in transmit power is greater, the harmonic gets attenuated.

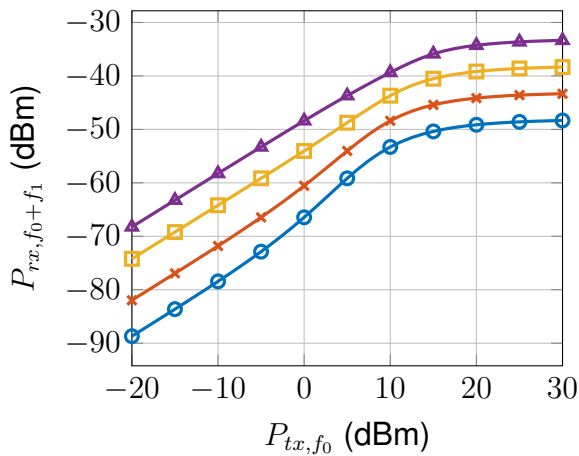
Finally figure 3.3c shows mostly behaviour that could be predicted from the mathematical model. It can be seen that when P_{tx,f_0} is increased with 10 dB, the power of the received harmonic P_{rx,f_0+f_1} also increases with 10 dB in the small signal region. One thing to note is that the spacing between the lines for the different transmit powers for the second transmitter P_{tx,f_1} is slightly larger than expected. Since following equation 2.4 it was expected that a 5 dB increase in transmit power should increase the power of the intermodulating term by 5 dB.



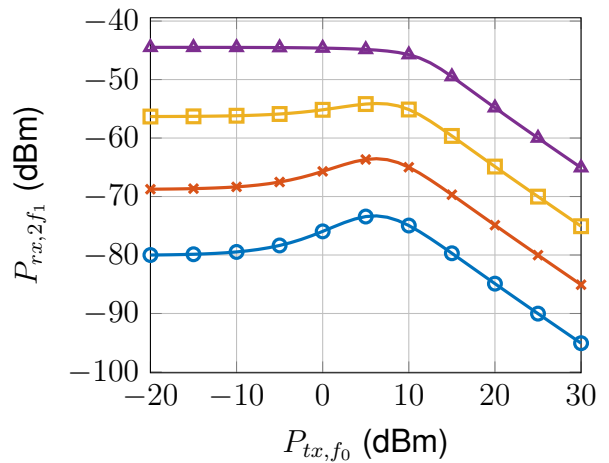
(a) 3D-sweep plotting received intermodulating power



(b) Power of harmonic from variable power transmitter



(c) Power of intermodulating harmonic



(d) Power of harmonic from constant power transmitter

Figure 3.3: Simulation results for two transmitters with unequal transmit powers

Chapter 4

Measurements

4.1 Measurement setup

In this project, measurements are limited to two transmitters which is enough for evaluating the model as shown in equation 2.1. Two signal generators were used to generate the carrier signals, and a spectrum analyzer was used to analyze the return signal from the tag. A list of the used equipment can be found in table 4.1. A schematic layout of the measurement setup can be seen in figure 4.1 and a picture can be seen in figure 4.2.

The design for the tag that was used for the measurement is described in [7]. The tag was designed for a fundamental transmit frequency of 2.9 GHz. The tag uses a SkyWorks SMS7630-040 diode as the non-linear element.

The distance between the antennas and the harmonic tag is 0.2 m. This distance was chosen as a trade-off between being far enough to not have reactive near-field effects and being close enough to have a strong signal at the harmonic tag without the need to use an external power amplifier. Due to limited transmit power, moving further would cause the received signal to quickly fall below the noise floor. The radiating near-field region is given by equation 4.1 [9]. In this equation r is the distance to the antenna, λ the wavelength and l the length of the antenna. Since the log periodic antenna used in the measurements has a length of 0.14 m and the used frequency of 2.9 GHz results in a wavelength of 0.103 m, the minimal distance for the radiating near-field region is 0.101 m.

$$\frac{2l^2}{\lambda} > r \geq 0.62\sqrt{\frac{l^3}{\lambda}} \quad (4.1)$$

The spectrum analyzer was used with a span of 30 kHz with 401 frequency points and a resolution bandwidth (RBW) of 300 Hz. The spectrum analyzer was set to average 10 sweeps in order to reduce the noise effect on the measurements. This value was

Type	Model
RF signal generator	Agilent 8267D
RF signal generator	Signal Hound SVG60A
Spectrum analyzer	Agilent E4404B
log-periodic antenna	WA5VJB 850-6500MHz, 6dBi
Helical antenna	5.8GHz, 12dBi

Table 4.1: Used measurement equipment

determined by inspecting at which value the measurements stabilised. The power was averaged in linear scale, instead of averaging in the logarithmic scale.

The experiments aim to replicate the simulations. To help with this, all equipment was controlled via MATLAB by sending Standard Commands for Programmable Instruments (SCPI). This ensures that the measurement equipment is always configured correctly and allows for repeatable experiments and storing all the results from the spectrum analyzer.

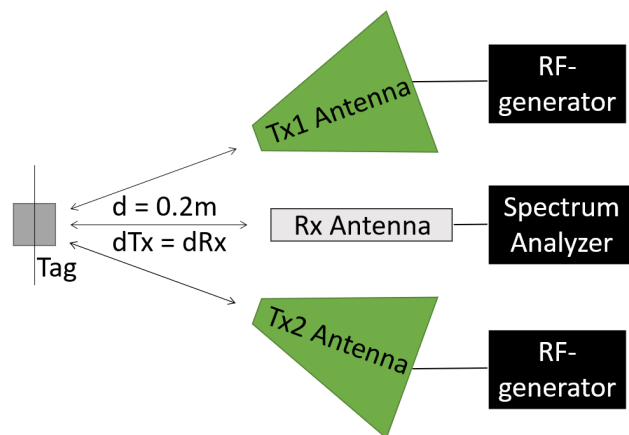


Figure 4.1: Schematic layout of the measurement setup



Figure 4.2: Picture of the measurement setup

4.2 Measurements with one transmitter

The first measurement taken was a power sweep with one transmitter. The power sweep was done from -10 dBm through 20 dBm, since lower values would cause the return signal to drop below the noise floor and 20 dBm was the limit of the RF-generator. The result of this measurement can be seen in figure 4.3a. In this figure we can already see the transition between the two regions of the two-region model. To better see this result, again a plot of the received power of the harmonic relative to the transmit power is made in figure 4.3b. Here, we can more clearly see that the measured response indeed starts to change from the quadratic behaviour to the quasi-linear behaviour. However, it can also be seen that below -100 dBm received power from the harmonic start to become less clean. In later measurements this phenomenon will also appear.

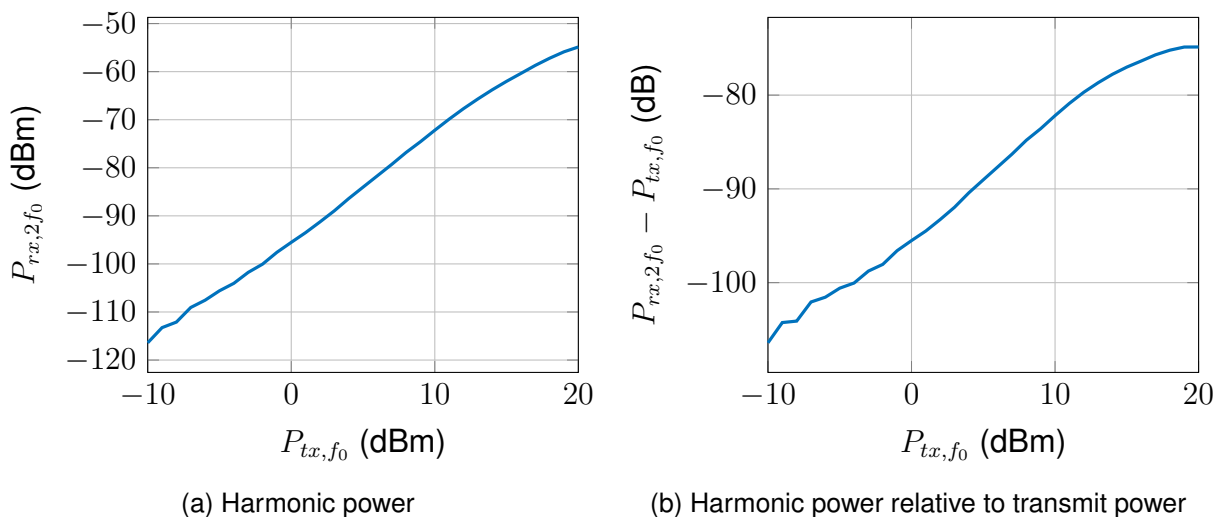


Figure 4.3: Measured received harmonic power as a function of transmit power

To verify how well these results meet theoretical expectations, they should be compared to the simulation results. The results from the simulations were added to the plots in figure 4.4a and 4.4b. However, these results are not that useful. It can be seen that the measured values are significantly lower than expected from the simulations. This is not unexpected for two reasons. The first is the method of calculating power losses in the transmission: for the antennas data from the specifications was used for the gain, which could be higher or lower than the real values. Especially since the measurements were not taken in the far-field region, but the radiating near-field region. Furthermore, the formula for the free space path loss does not account for reflections. Secondly, the lower values could be expected due to the assumptions made by the model: the model assumed perfect matching of the tags antenna, diode and inductive loop at all operating frequencies. In reality, this is unrealistic. Imperfect matching would also cause loss of power in the harmonic tag.

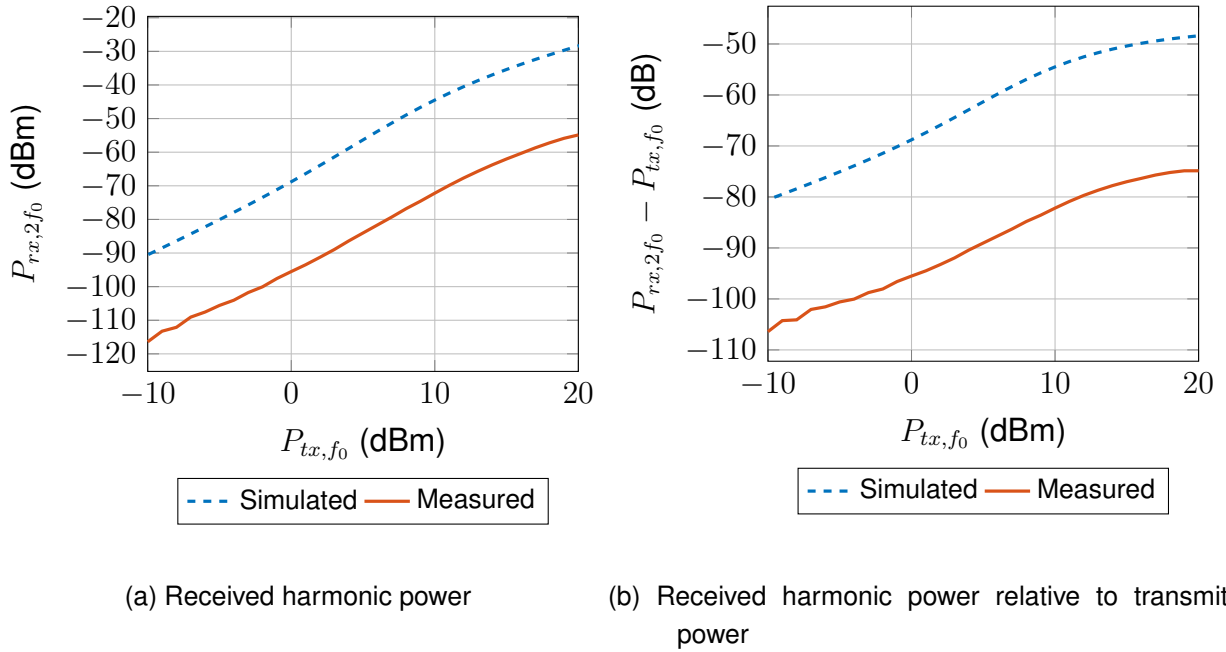


Figure 4.4: Direct comparison between measured and simulated data

However, to validate the model it is more important if the overall shape of the curve aligns with expectations. Therefore, to better compare the simulations results to the measurements, the simulation results were fitted onto the measurement results by moving them on the X- and Y-axis. A move in the X-axis would translate into a bigger loss in transmission from the RF-generator to the harmonic tag than expected and a move in the Y-axis would translate into a bigger loss in transmission from the harmonic tag to the spectrum analyzer than expected.

MATLAB was used to fit the simulations to the measurement results. For this, an error function was defined that can be seen in equation 4.2. In this equation X_{meas} is the power level at which measurements were taken, Y_{meas} is the corresponding measured value for received harmonic power, f_{model} represents the function that maps X values to Y values in the simulations and α and β are the variables that can be tuned to minimize the error. Since simulation also consists of discrete points, linear interpolation was used to estimate received harmonic power values between points. The high power at the end of the error function was chosen to prefer an evenly distributed average error to a bigger error that only exists in a smaller part of the curve.

$$E = (|f_{model}(X_{meas} - \alpha) - Y_{meas} + \beta|)^4 \quad (4.2)$$

The optimization toolbox was used to minimize this error function. It was decided to fit

the results from 0 dBm through 20 dBm for two reasons. First, in this region the line was starting to curve, which is the more interesting behaviour to use for the fit than the straight line. Secondly, it was observed that the measurement results in the lower region are noisier, which resulted in a poorer fit. The results of the function fit can be seen in figure 4.5a and 4.5b.

When comparing simulations and measurements in figure 4.5a and 4.5b, it can be seen that they are extremely close and follow each others curvature.

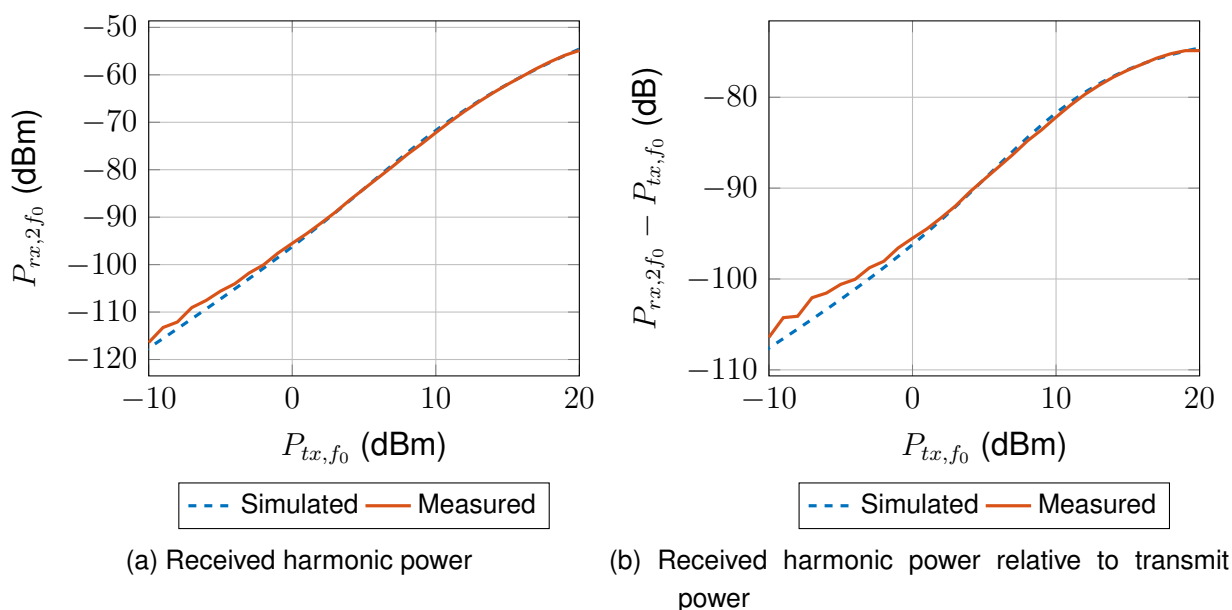


Figure 4.5: Fitted comparison between measured and simulated data ($x = 1.19$ dB, $y = -24.64$ dB)

4.3 Measurements with two transmitters

The second measurement was with two transmitters sweeping with equal power. During measurements it was noticed that with two transmitters used, setting the same output power did not always result in the same measured harmonic power. This is likely a combination of differences in location of antennas, cables and different calibration between the two generators. To compensate for this, precautions were taken to minimize the error between the harmonics. This was done by comparing received power at the second harmonic for each transmitter separately, and then adjusting one of them to compensate for the difference. This was done once at the beginning of the power sweep to set a coarse compensation value and then adjusting the output power before each measurement so that the two measured powers are as close as possible.

The result of the measurements can be seen in figure 4.6a. This figure looks very close to what is expected from the model. Figure 4.6b was plotted to show the difference between the harmonics and the intermodulating term. On average the difference between the two harmonics and the intermodulating term was found to be 5.48 dB. While slightly lower than the 6dB value expected from the model in section 2.3, it was expected from the simulation results. As shown in chapter 3 figure 3.2b, when transitioning between the small signal and large signal region, the gap between the harmonics and the intermodulating term first narrows before becoming wider again. These measurements were taken right around the part where the gap narrows. However, an important conclusion is that for the entire range of input powers the intermodulating term is present and at least 5 dB stronger than the other harmonics.

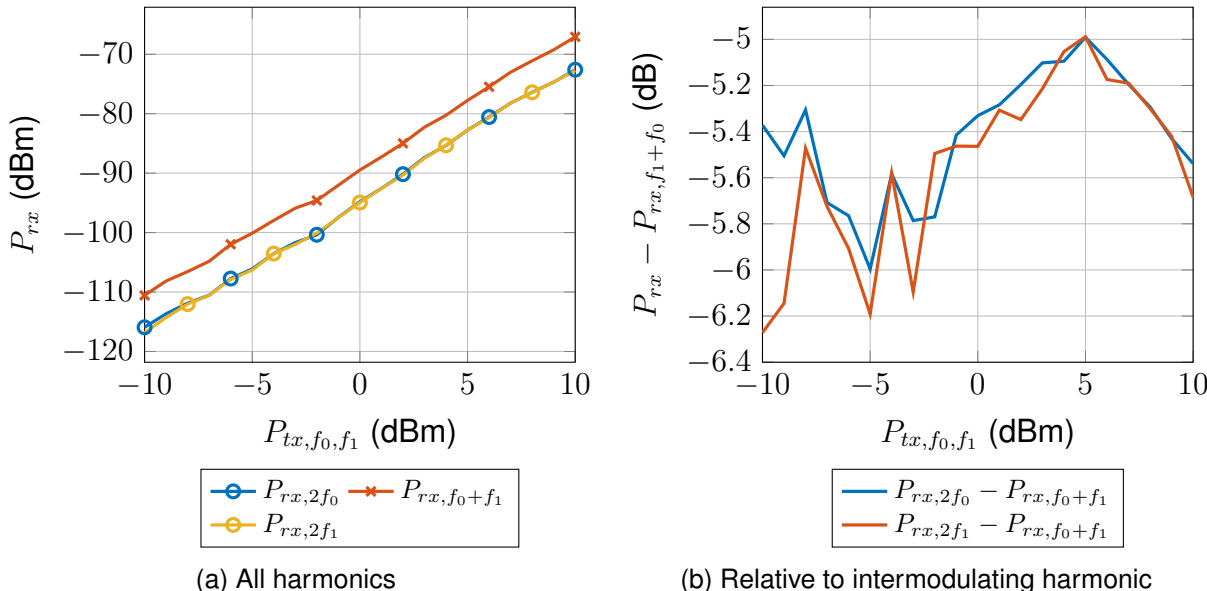


Figure 4.6: Measured received harmonic power as a function of transmit power with two transmitters

To better compare the measurements to the simulation results, they were plotted together in figures 4.7a and 4.7b. The same fitting technique as described for the single power sweep was applied, where the upper region of the curve was used for the fitting process. However, for this fit all three curves were taken into account. It can be seen that the measurements follow the simulations. We also see again that at the lower power levels the measured powers are higher than the expected values.

However, when we examine figure 4.7b we can immediately see that the fitting algorithm has not given the best fit. While the fit looked good in figure 4.7a, here it can be seen that the shift on the X-axis that was applied is incorrect. While the shift in the X-axis of 1.27 has moved the curves closer together, a higher value would be required to let the curves overlap. This shows how difficult it is to compare the results: even though results may

look to fit, it might turn out a slightly different fit would have been more optimal. However, since the shift was relatively minor it is still safe to conclude that the measurements seem to follow the simulations remarkably well.

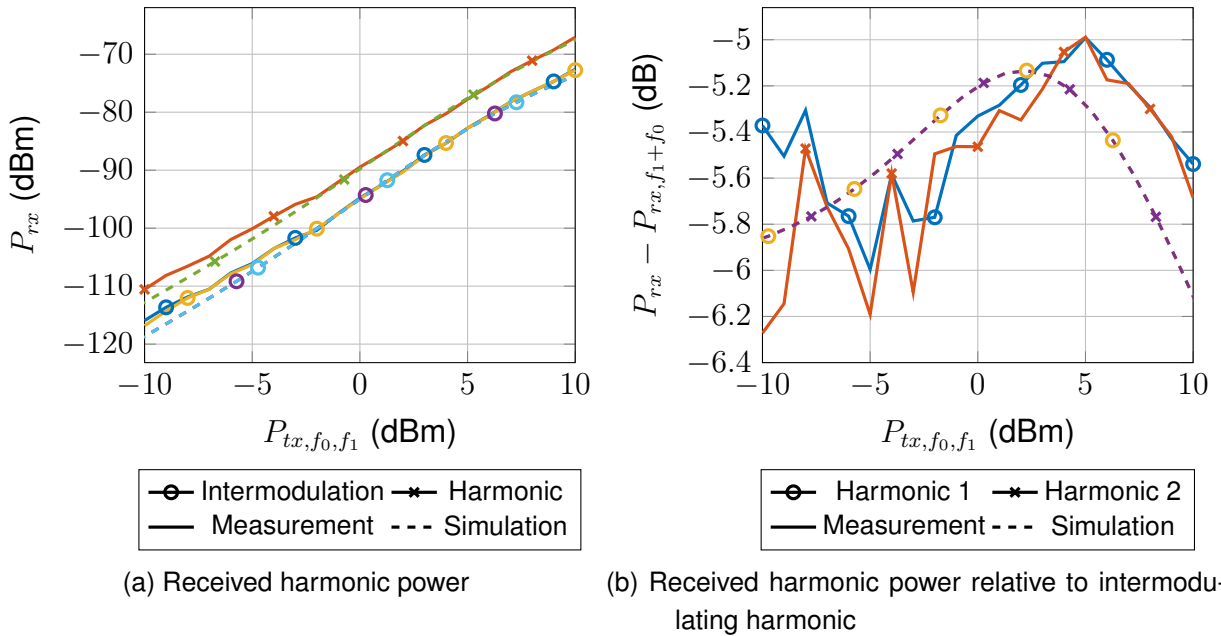
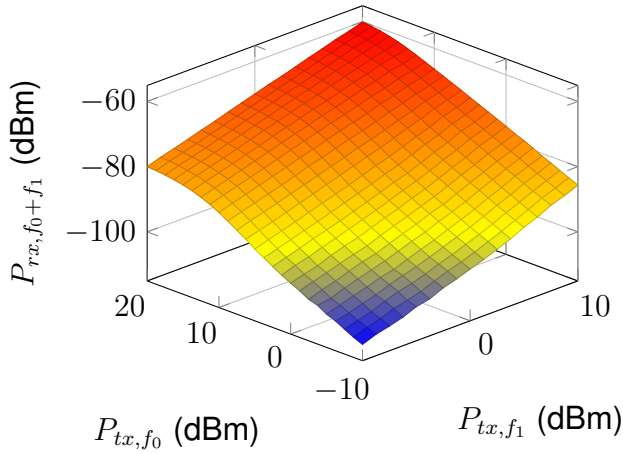


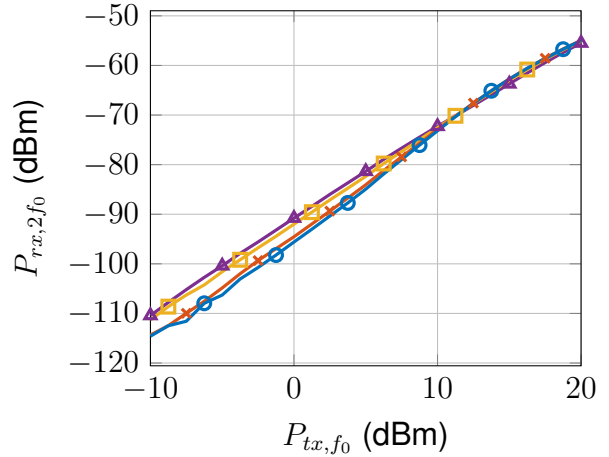
Figure 4.7: Fitted comparison between measured and simulated data ($x = 1.27$, $y = -26.03$)

Finally, the measurements with unequal transmit powers were performed. The resulting surface plot can be seen in figure 4.8a. Furthermore, slices of these measurements were taken for the three harmonic terms. Figure 4.8b shows the power of the harmonic from the first transmitter $P_{rx,2f_0}$, figure 4.8c shows the power of the intermodulating harmonic P_{rx,f_0+f_1} , and figure 4.8d shows the power of the harmonic from the second transmitter $P_{rx,2f_1}$. For all these plots the X-axis is the power set to the first transmitter P_{tx,f_0} , with plots for the different power levels of the second transmitter P_{tx,f_1} . In these three plots, we can see the attenuation of the weaker harmonic that was also found during the simulations.

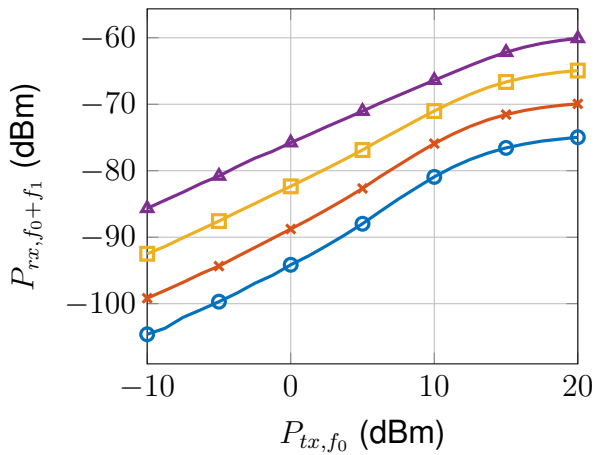
To compare these measurements to the simulation they were again fitted to each other. However, for these measurements the methodology of fitting was slightly changed. Since we now have two variables instead of one, surfaces were fitted onto each other instead of curves. The surfaces of the three different harmonics were all taken into account. The result of this fit can be seen in figures 4.9a, 4.9b and 4.9c. In figure 4.9a and 4.9b it can be seen that the measurements follow the simulations extremely well. There are only small deviations, especially in the lower power regions. The same trend continues in figure 4.9c. However, in this figure the difference in power level in the low power region is more significant than the other plots.



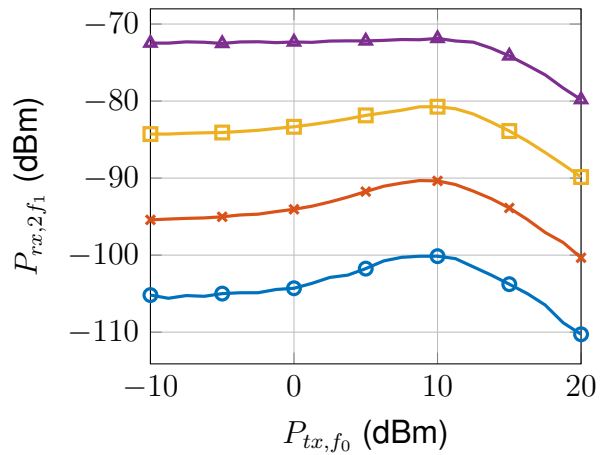
(a) 3D-sweep plotting received intermodulating power



(b) Power of harmonic from variable power transmitter

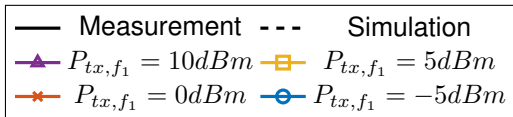
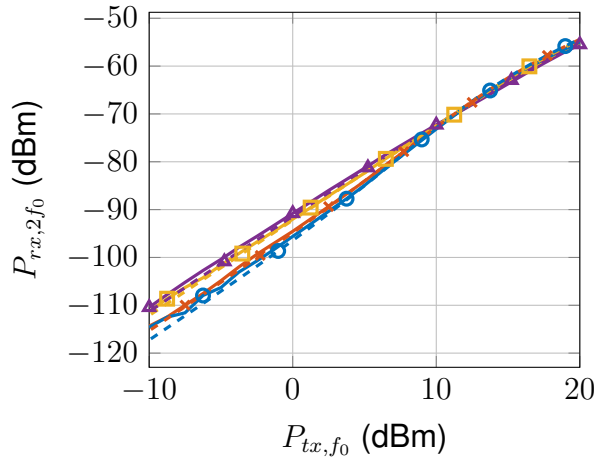


(c) Power of intermodulating harmonic

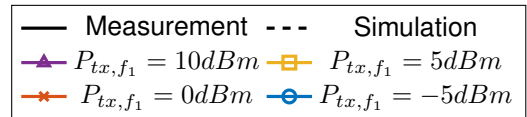
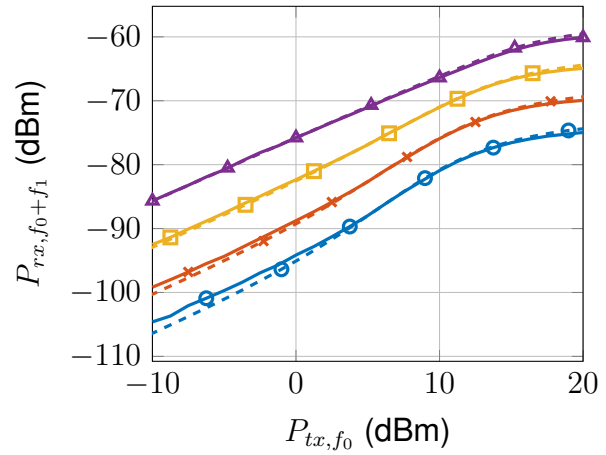


(d) Power of harmonic from constant power transmitter

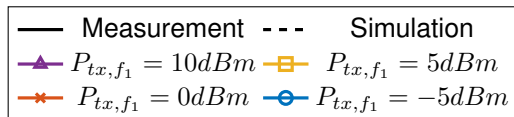
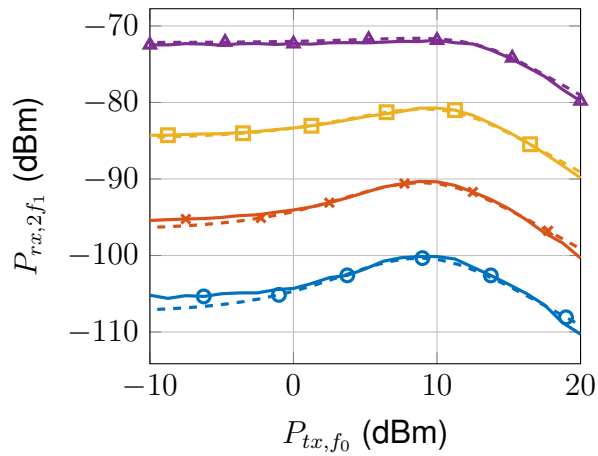
Figure 4.8: Measurement results for two transmitters with unequal transmit powers



(a) Power of harmonic from variable power transmitter



(b) Power of intermodulating harmonic



(c) Power of harmonic from constant power transmitter

Figure 4.9: Fitted comparison between measured and simulated results for two transmitters with unequal transmit powers ($x = 2.99$, $y = 2.39$, $z = -22.30$)

4.4 Modulated carrier

Finally, one measurement was done with a modulated carrier to show the effect of using two transmitter in a configuration closer to a practical setup. To do this, one transmitter was set to transmit chirps with a bandwidth of 1 kHz and a period of 100 ms. To get an indication of the transmit power, the average power was taken over 100 sweeps. The result can be seen in figure 4.10. It can be seen that the three harmonics are created. However, it can also be seen that the bandwidths are not as was expected. However, this is highly dependent on the used way of defining the upper and lower bound of the bandwidth. If only the top of the bandwidth block was used, the bandwidth would be closer to the expected values. Furthermore, the power of the different terms was measured by integrating the linear values from the lower through the upper bound for the different terms. A power of -71 dBm, -87 dBm, and -91 dBm was calculated for the lower harmonic, intermodulating harmonic and higher harmonic, respectively. Noteworthy is that the power of the unmodulated harmonic is far higher than the other harmonics. For these values it must be noted that the measurement setup is not optimal to measure the power of the modulated signals. By averaging over a large number of sweeps the frequency block can become visible but does not give an accurate representation of the power. Furthermore, the relatively high resolution bandwidth (RBW) of 300 Hz also causes frequency points to overlap. However, when taking this into account we can still see that the intermodulating term contains more power and has a lower bandwidth compared to the harmonic of the modulated transmitter.

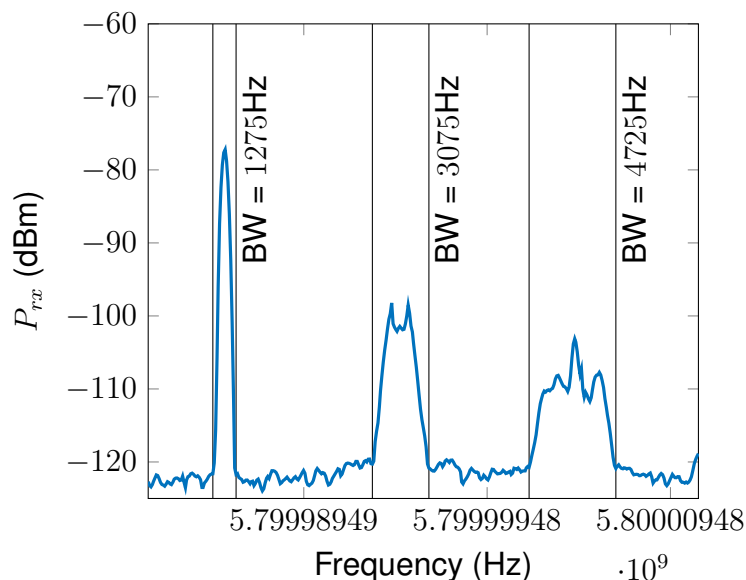


Figure 4.10: Measurement with modulated carrier

Chapter 5

Conclusion and Outlook

The goal of this paper was to experimentally evaluate a mathematical model for harmonic radar tags. For this, first a foundation was laid out explaining the principle of harmonic radar. Then a mathematical model for harmonic tags and a basic theory behind using auxiliary transmitters were presented. To be able to evaluate the model, the results of simulations were used to form a test benchmark for the measurement results. Using a setup consisting of two RF generators and a spectrum analyzer, the response of a harmonic tag was measured under different conditions.

When comparing the results of these measurements to the simulations, it can be concluded that the model is accurate enough to be used for modelling both harmonic tags and intermodulation operation of harmonic tags. It provides a viable tool that can be used to model, design and implement harmonic radar systems. This is because none of the differences between measurements and simulations influence the broader picture of what the model is used for. The measurements also confirm the viability of using auxiliary transmitters in the way the model predicted. The intermodulating term was present for all input power levels with at least 5 dB more power for equal transmit powers.

The main limitation of the model is that all simulations predicted the power of the harmonics too high compared to the measurements. The simulation results needed a down adjustment between 22 and 26 dB to correspond with the measurements. While this is important to keep in mind when using the model, it would only cause problems by overestimating the operating range. Furthermore, there were some smaller differences between harmonics or certain behaviour that is less prominent in the measurements than they are in the simulations. However, these differences are so minor that they can be discarded in practice.

The presented results also lead to some new insights for future design of harmonic radar systems that utilize auxiliary transmitters. Systems that use a modulation scheme where

$x \neq x^2$, such as radar chirps, normally rely on the intermodulating term as their return signal. However, a situation could occur where the modulated transmitter is close to the tag, but the auxiliary transmitter is far away. In this case, as can be seen in figure 4.8a, the intermodulating harmonic would be weak due to the low power received from the auxiliary transmitter. The system would then perform worse compared to just using the harmonic of the modulated signal. This could be prevented in two ways. First is making sure that the transmitters are relatively close to each other. However this would partially negate the advantage of two transmitters. A second option is the usage of a split setup: the receiver can decide to either use the harmonic of the modulated signal, or the intermodulating harmonic depending on the received power level. It could even be decided to try and use both of these signals together in a combined manner.

To conclude, this report showed the results of an experimental evaluation of harmonic tag operation in the presence of multiple transmitters. The goal was to address two research questions. The first research question was:

1. *"How well does the mathematical model of a harmonic tag describe tag operation with multiple transmitters?"*

The presented results indicate that the theoretical model describes the response of the harmonic tag very well after an adjustment for the power level mismatch.

The second question was:

2. *"How to design harmonic radar systems to best utilize a multiple transmitter configuration?"*

The results show that it is a good approach to design a system to receive and process both the harmonic and intermodulating components of the return signal. This would allow for optimal operation in most situations.

Bibliography

- [1] A. Mishra and C. Li, "A review: Recent progress in the design and development of nonlinear radars," *Remote Sensing*, vol. 13, no. 24, p. 4982, Dec. 2021. [Online]. Available: <https://doi.org/10.3390/rs13244982>
- [2] H. Aniktar, D. Baran, E. Karav, E. Akkaya, Y. S. Birecik, and M. Sezgin, "Getting the Bugs Out: A Portable Harmonic Radar System for Electronic Countersurveillance Applications," *IEEE Microwave Magazine*, vol. 16, no. 10, pp. 40–52, nov 2015. [Online]. Available: <http://ieeexplore.ieee.org/document/7298555/>
- [3] E. Cant, A. Smith, D. Reynolds, and J. Osborne, "Tracking butterfly flight paths across the landscape with harmonic radar," *Proceedings of the Royal Society B: Biological Sciences*, vol. 272, no. 1565, pp. 785–790, Apr. 2005. [Online]. Available: <https://doi.org/10.1098/rspb.2004.3002>
- [4] J. Olofsson, T. Forssen, G. Hendeby, I. Skog, and F. Gustafsson, "UAS-supported digitalized search-and-rescue using harmonic radar reflection," in *2020 IEEE Aerospace Conference*. IEEE, Mar. 2020. [Online]. Available: <https://doi.org/10.1109/aero47225.2020.9172655>
- [5] A. Lavrenko, S. Pawson, and J. Cavers, "On the use of additional transmitters for increasing detection range in harmonic radar," in *2019 13th International Conference on Signal Processing and Communication Systems (ICSPCS)*, 2019, pp. 1–8.
- [6] A. Lavrenko and J. Cavers, "Two-region model for harmonic radar transponders," *Electronics Letters*, vol. 56, no. 16, pp. 835–838, Aug. 2020. [Online]. Available: <https://doi.org/10.1049/el.2020.0779>
- [7] A. Lavrenko, B. Litchfield, G. Woodward, and S. Pawson, "Design and Evaluation of a Compact Harmonic Transponder for Insect Tracking," *IEEE Microwave and Wireless Components Letters*, vol. 30, no. 4, pp. 445–448, apr 2020. [Online]. Available: <https://ieeexplore.ieee.org/document/9006943/>
- [8] S. Inc., "Skyworks sms7630 series data sheet." [Online]. Available: <https://www.skyworksinc.com/en/Products/Diodes/SMS7630-Series>

- [9] C. A. Balanis, "Radiation Power Density," in *Antenna Theory - Analysis and Design*, 4th ed. John Wiley & Sons, 2016, ch. 2.3.
- [10] —, "Half-Wavelength Dipole," in *Antenna Theory - Analysis and Design*, 4th ed. John Wiley & Sons, 2016, ch. 4.6.